Behavior of moving droplet on inclined containment wall: Experiment and model validation

Fangnian Wang, Meng Zhao *

Institute for Applied Thermofluidics (IATF), Karlsruhe Institute of Technology (KIT), Germany

ARTICLE INFO

Keywords:
Moving droplet
Experiment
Validation
Droplet velocity
Containment wall

ABSTRACT

Understanding the behavior of moving droplet on inclined containment wall is significant to evaluate condensation heat and mass transfer, aerosol wash-down by condensate flow, etc. The models describing moving droplet, such as the onset of motion, the droplet velocity and the flow pattern transition criterion from droplet to rivulet are presented. Concerning the droplet velocity model, the flow field inside droplet and the dynamic contact angle model are considered to evaluate the viscous force and surface tension force respectively acting on fast moving droplet. A new experiment of water droplets moving on inclined surface coated with decontamination paint, DRISE, is performed with the *Re* number range $56<Re<1700$. The model for the onset of the droplet motion matches the DRISE data very well. At high *Re* number, the new developed droplet velocity model on the tilted surface and the criterion of the transition from droplet to rivulet are well validated with the data from the DRISE experiment and the experiment from open literature.

1. Introduction

Dropwise condensation is a common fundamental phenomenon and widely used in engineering applications. This type of condensation is characterized by a significantly high heat transfer (Rose and Glicksman, 1973; De la Rosa, et al., 2009). The condensate droplet departuring from the wall and sliding down the surface are the most important effects, which disrupt the continuity of the noncondensable gases barrier. Dropwise condensation can take place in the very high part of the inclined containment structures which is much more efficient than film condensation. At the beginning of condensation the droplet generates on inclined cooling surface and grows up until its volume reaches a threshold (the onset of motion), beyond which the droplet starts to move downward the wall surface. Droplet grows up during its movement, until the transition criterion (from droplet to rivulet) is satisfied. After the transition, rivulet forms and develops until the structure is fully covered by film. Therefore, the investigation of the dynamic behavior of droplet on inclined solid surfaces is essential to understand and improve the application performance in relevant engineering, e.g. the nuclear passive containment cooling systems, aerosol wash-down by condensate flow (Wang and Cheng, 2019, 2020).

To describe a moving water droplet, the onset of droplet motion is the first issue to be considered. The retention of water droplet on inclined surface with respect to gravity and surface tension, is particularly significant for static droplet on the verge of droplet sliding (Furmidge, 1962). The surface properties are among the most important factor controlling the retention of water droplet on solid surfaces. Previous efforts (Brown et al., 1980; Dussan, 1985; Extrand and Kumagai, 1995; ElSherbini and Jacobi, 2006) calculated the retentive force with different assumptions of droplet contact line contour. Brown et al. (1980) found the shapes of given volume and density droplets on an inclined surface is a circular wetted contact area by solving the Young-Laplace equation. Dussan (1985) analyzed the ability of a small droplet stick on an inclined solid surface. The results identified the critical size (or volume) and the wetted area of the droplet with the assumption that the contact line contour is parallel-sided and the value of the contact angle hysteresis is small. Extrand and Kumagai (1995) studied the droplet shape and the retention on a tilted plane on different substrate surfaces experimentally. The results revealed that the droplet exhibiting advancing and receding contact angles when the droplet is still on a sloped surface. The contact angle hysteresis ranged from 9° to 66°, depending on the substrate and the liquid. ElSherbini and Jacobi (2006) investigated the retention force and droplet parameters for droplets on the verge of sliding on inclined surfaces. The retention force is found to be insignificantly affected by the aspect ratio of its contour. Ryley and Ismail (1978) experimentally investigated the water droplet on polytetralluoroethylene (PTFE) coated sloped surface (equilibrium contact

* Corresponding author at: Karlsruher Institute of Technology (KIT), Institut for Applied Thermofluidics (IATF), Kaiserstraße 12, 76131 Karlsruhe, Germany.
E-mail address: meng.zhao@kit.edu (M. Zhao).

Nomenclature

Symbol Explanation, Unit, General

A	contact (wet) area of droplet, m^2
Bo	Bond number, -
Bo_c	critical Bond number where droplet start moving, -
Bo_t	Bond number where transition happens, -
Ca	Capillary number, -
$c_1/c_2/c_3/c_4$	functions of equilibrium contact angle , -
c_5/c_6	constant value, -
F_g	gravitational force of droplet, N
F_M	equivalent Marangoni force acting on droplet, N
F_σ	surface tension force of droplet, N
$F_{\sigma,A}/F_{\sigma,R}$	advancing/receding component of surface tension force of droplet, N
F_τ	viscous forces of droplet bulk part, N
$F_{\tau,w}$	viscous forces of droplet wedge part, N
g	gravity acceleration, 9.8 , m/s^2
g_{iv}/g_v	functions of contact angle, -
k	factor of droplet surface tension force, -
L_a	apparent (macroscopic) length of droplet, m
L_s	microscopic cut-off length scale of droplet, m
P	droplet contact area perimeter, m
Re	Reynolds number, -
r	radius of droplet, m
r_t	radius of droplet where transition happens, m
u	droplet velocity, m/s
V	droplet volume, m^3
V_t	critical volume where transition happens, m^3
We	Weber number, -
Δy	droplet height in y- direction, m

Greek symbols

α	inclination angle, °
δ	layer thickness, m
θ_e	equilibrium contact angle, °
$\theta_{d,A}/\theta_{d,R}$	dynamic advancing and receding contact angle, °
θ_s/θ_d	static/dynamic contact angle, °
$\theta_{s,A}/\theta_{s,R}$	static advancing and receding contact angle, °
θ^*	intermediate variable in the Cox, 1998 model, °
μ	dynamic viscosity, Pa·s
ρ	water density, kg/m^3
σ_{LG}	surface tension between water and air, N/m
$\Delta\sigma_{LG}$	surface tension change caused by temperature gradient, N/m

angle of 20°, less than water droplet on decontamination paint coated surface) as well as water droplet over an alkyl ketene dimer (AKD) surface (equilibrium contact angle of 165°, more than water droplet on decontamination paint coated surface) in reference (Pierce et al., 2008). Goodwin et al. (1988) obtained experimental data for the critical volume of the onset of droplet motion over a range of relevant parameters. The validation revealed the Dussan, 1985 model was in good quantitative agreement with the experimental data. The importance for us is that the current model of the onset of droplet motion is probably valid and there is no experimental data for the water droplet on decontamination paint surface.

Once the droplet motion starts, the droplet moves at constant velocity in steady state condition. The droplet velocity is strongly dependent on the internal flow field of the droplet. For sliding slowly droplets, a classic linear scaling law of droplet velocity is proposed and validated in references (Podgorski et al., 2001; Kim et al., 2002). The lubrication theory is usually assumed to scale the velocity gradient for droplet sliding at low Re number (e.g. $Re < 1$). When droplet moves fast down on inclined surface, its velocity model needs to consider the inertial effect (Puthenveettil et al., 2013). The advancing contact angle is relatively large and there is a rotation flow inside the droplet. The early criterion for the distinguishing of droplet flow patterns (lubrication and rotation) depends on the dynamic advancing contact angle being less or greater than 90° (Allen and Benson, 1975). There has been a long-standing debate on these two flow patterns inside droplet sliding down on an inclined surface. High-speed visualization coupled with image analysis of the water droplet moving down on an inclined surface has been investigated recently (Sakai et al., 2006; Song, 2008; Suzuki et al., 2008). Experimental researches propose that the velocity of the top surface of the droplet is greater than the bottom interface motion, the rotation flow inside the droplet appears. Some research indicates there is a mixture of flow pattern (Song, 2008; Takahashi et al., 2018). Influence factors to determine the droplet flow pattern are summarized: surface properties (rotation with high hydrophobicity), viscosity ratio of the droplet fluid to the ambient immiscible fluid (rotation with high viscosity ratio), dynamic contact angle (rotation with large advancing contact angle, and small contact angle hysteresis), and so on. Wadgaonkar et al. (2015) develops a theoretical criterion, co called 'slip Reynolds number' to predict the rotating droplet moving down on an inclined surface. Our previous studies (Wang et al., 2018; Wang and Cheng, 2019) investigated the droplet velocity model at high droplet Re number. The droplet velocity model considers the change of dynamic contact angle hysteresis when the droplet moves fast, in order to estimate the resistance accurately caused by surface tension. However, the model is assumed that the droplet height equals the droplet radius, which results in underestimating the viscous force.

Moreover, few studies of the flow pattern transition from droplet to rivulet are presented in literatures. Puthenveettil et al. (2013) provide the velocity thresholds of water and mercury droplets on glass surface, but these thresholds are different from case to case. A generic transition criterion that can be feasible to estimate the transition from water droplet to rivulet on containment structure surface, is proposed in our previous research (Wang and Cheng, 2019).

In this paper, the velocity model of droplet moving at highRe is updated in detail with the consideration of internal flow field and dynamic contact angle. A new fundamental droplet experiment is set up to investigate the behavior of moving droplet on inclined containment wall. The onset of motion, the droplet velocity at high Re, and the transition criterion are validated by the new experiment.

2. Model description

2.1. Onset of droplet motion

Depending on the applications of the condensation droplet, it is expected that the droplets to flow downward on the solid surface. The gravity and surface tension are important to identify the conditions whether the droplet will rest on the surface (Furmidge, 1962). As shown in Fig. 1, for a given volume of droplet, due to a further increase of inclination angle, the droplet starts to move down the surface. The droplet size at the onset of motion (velocity is 0) is determined with the force balance:

$$F_g \sin\alpha = F_{\sigma,R}\cos\theta_{s,R} \quad F_{\sigma,A}\cos\theta_{s,A} \tag{1}$$

The component of the gravitation parallel to the surface is:

$$F_g \sin\alpha = V\rho g \sin\alpha \tag{2}$$

The surface tension force parallel to the surface, denoted by F_σ, is:

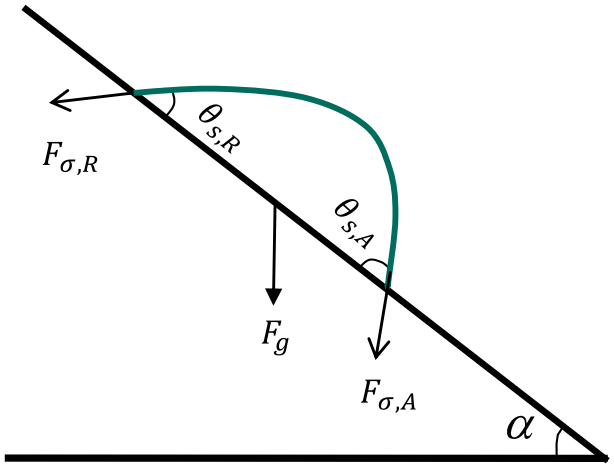

Fig. 1. Onset of droplet motion.

$$F_\sigma = F_{\sigma,R}\cos\theta_{s,R} \quad F_{\sigma,A}\cos\theta_{s,A} = k \cdot 2r\sigma_{LG}\left(\cos\theta_{s,R} \quad \cos\theta_{s,A}\right) \tag{3}$$

where ρ is the droplet density, g is the acceleration of gravity, V is the droplet volume, α is the surface inclination angle, which is the angle between the surface and the horizontal direction. r is the radius of droplet wetting area, σ_{LG} is the surface tension of the gas–liquid interface (here, air–water interface),$\theta_{s,A}$ and $\theta_{s,R}$ are the apparent static advancing and receding contact angle respectively.

The factor k of the droplet surface tension force depends on the contact line contour of the droplet, as shown in Table 1. Previous efforts (Brown et al., 1980; Dussan, 1985; Extrand and Kumagai, 1995; ElSherbini and Jacobi, 2006) indicate the factor k is in values between 1.0 and 1.57, because of different assumptions and predictions of the droplet contact line contour.

The ratio of the gravitation force to the surface tension force Bond number$Bo = \frac{\rho V^{2/3} g \sin\alpha}{\sigma_{LG}}$, is widely adopted to estimate the stability of rest droplets on inclined surface. For a given surface slope, the onset of droplet motion occurs at a critical droplet volume, so that the surface tension resistance is just overcome by the gravitation. The Bond number at the onset of motion, so called the critical Bond number Bo_c depends on the static advancing and receding contact angles. ElSherbini and Jacobi (2006) proposed another formula without the limitation of the contact angle hysteresis:

$$Bo_c = \frac{24}{\pi^3}\left(\frac{24}{\pi}\right)^{1/3} \frac{\left(\cos\theta_{s,R} \quad \cos\theta_{s,A}\right)\sin\frac{\theta_{s,A}+\theta_{s,R}}{2}}{\left(2 \quad 3\cos\frac{\theta_{s,A}+\theta_{s,R}}{2} + \cos^3\frac{\theta_{s,A}+\theta_{s,R}}{2}\right)^{1/2}} \tag{4}$$

Once the critical Bond number Bo_c is acquired by knowing the static contact angles, for given inclination and fluid properties further, the droplet volume at its onset of motion is obtained.

Using force balance is the most common mothed to analyze the onset of droplet motion. Under condensation condition, the droplet motion couples with the heat and mass transfer. At beginning, the droplet generates on the dry cold surface and grows up until its volume reaches the threshold (the droplet critical size), beyond which the droplet starts to move downward the wall surface. The heat and mass transfer process influences the speed to reach the critical size. Furthermore, heat and mass transfer process dominates the water temperature and the temperature gradient that lead to a change of surface tension.

Table 1
Factor k of droplet surface tension force.

Author	$k$value	contour assumption
Brown et al., 1980	$\pi/2$	circular
Dussan, 1985	1.0	parallel-sided
Extrand and Kumagai, 1995	$4/\pi$	circular
ElSherbini and Jacobi, 2006	$48/\pi^3$	elliptical

2.2. Previous droplet velocity mode

When the droplet volume or inclination angle becomes larger than the threshold value of the onset of motion, the droplet sliding occurs. The droplet could move at constant velocity in steady state condition. Except the gravitation force and the surface tension force, the viscous force should be also considered to evaluate the droplet moving velocity, as shown in Fig. 2.

The viscous force at the solid–liquid interface is determined by the liquid viscosity and the velocity gradient there. The viscous force at the gas–liquid interface is neglected here. The viscous force at the solid–liquid interface is determined by the liquid viscosity and the velocity gradient there. This viscous dissipation consists of a flat bulk (central) part mainly governed by gravity and a wedge (edge) part where the capillarity takes effect (Kim et al., 2002).

When the droplet slides at low Re ($Re < 1$) number, the velocity field in the bulk part can be assumed to obey the lubrication approximation, whereas the velocity field in the wedge part must be described using the Stokes equation. De Gennes (1985) and Kim et al. (2002) think that the viscous forces $F_{\tau,w}$ acting on the wedge part of droplet near the contact line, as shown in Fig. 2, dominates viscous dissipation when the droplet diameter is smaller than the capillary length $\sqrt{\sigma_{LG}/\rho g}$. When the droplet diameter is much larger than capillary length, the viscous force F_τ from the shear stress associated with the bulk part of droplet, dominates the viscous dissipation.

The force balance of the moving droplet in the moving direction is:

$$F_g \sin\alpha = F_\sigma + F_{\tau,w} + F_\tau \tag{5}$$

where F_σ is the component of the surface tension force parallel to the surface, expressed as in Eq. (3). According to the knowledge of the literature (Kim et al., 2002; Puthenveettil et al., 2013), the viscous forces $F_{\tau,w}$ acts on the wedge part can be expressed as:

$$F_{\tau,w} = 4\mu u P c_1(\theta_e)\ln\left(\frac{L_a}{L_s}\right) \tag{6}$$

where $P = 2\pi r$ is the droplet contact area perimeter. Sliding droplet shape usually can be approximated as a spherical cap. The apparent (macroscopic) length L_a, is an order of 1 mm while the microscopic cut-off length scale L_s is the slip length of a few molecular lengths with the order of 100 nm. Here $\ln\left(\frac{L_a}{L_s}\right)$ is approximated as 9.2. $c_1(\theta_e)$ is a function

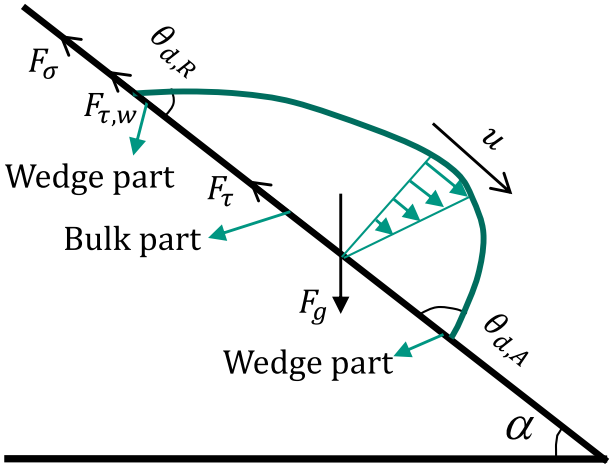

Fig. 2. Forces acting on moving droplet on inclined surface.

of equilibrium contact angle, which is derived by Kim et al. (2002) and Puthenveettil et al. (2013) based on the Stokes flow velocity field solution.

$$c_1(\theta_e) = \frac{(1 \quad \cos^2\theta_e)}{(\theta_e \quad \sin\theta_e\cos\theta_e)} \tag{7}$$

The viscous force F_τ of the bulk part of droplet depends on droplet internal velocity gradient close to the solid surface:

$$F_\tau \propto \mu A \frac{u}{\Delta y} = \mu u V^{1/3} c_2(\theta_e) \tag{8}$$

where$u/\Delta y$ is the internal velocity gradient since the lubrication theory is usually used to scale the velocity gradient. $A = \pi r^2$ is the droplet contact area while Δy is the height (thickness) of the droplet. Both of them are dependent on the droplet shape, e.g. the contact angle. The droplet radius is (Meric and Erbil, 1998):

$$r = \left(\frac{3V}{\pi} \frac{\sin^3\theta_e}{2 \quad 3\cos\theta_e + \cos^3\theta_e}\right)^{1/3} \tag{9}$$

with the equilibrium contact angle $\theta_e = (\theta_{s,A} + \theta_{s,R})/2$. The average droplet height can also be approximated as:

$$\Delta y = \left(\frac{3(1 \quad \cos\theta_e)V}{\pi(2 + \cos\theta_e)}\right)^{1/3} \tag{10}$$

The function of equilibrium contact angle$c_2(\theta_e)$ can be approximated by substituting droplet geometry:

$$c_2(\theta_e) = \frac{A}{\Delta y V^{1/3}} = \left(\frac{\pi\sin^3\theta_e}{2 \quad 3\cos\theta_e + \cos^3\theta_e}\right)^{2/3} \left(\frac{3(2 + \cos\theta_e)}{1 \quad \cos\theta_e}\right)^{1/3} \tag{11}$$

Substituting the viscous forces $F_{\tau,w}$ and F_τ into the force balance Eq. (5):

$$\rho V g \sin\alpha = 2kr\sigma_{LG}\left(\cos\theta_{s,R} \quad \cos\theta_{s,A}\right) + 4\mu u P c_1(\theta_e) \ln\left(\frac{L_a}{L_s}\right) + \mu u V^{1/3} c_2(\theta_e) \tag{12}$$

Both sides of the equation divided by $\sigma_{LG} V^{1/3}$ and expressed with *Bo* number:

$$\frac{\mu u}{\sigma_{LG}} \left(\frac{4Pc_1(\theta_e)\ln\left(\frac{L_a}{L_s}\right)}{V^{1/3}} + c_2(\theta_e)\right) = Bo \quad Bo_c \tag{13}$$

$$Ca \cdot c_3(\theta_e) = Bo \quad Bo_c \tag{14}$$

The definition of the dimensionless parameter Capillary number is $Ca = \frac{\mu u}{\sigma_{LG}}$. Substituting the expressions of droplet perimeter P, droplet volume V and $\ln\left(\frac{L_a}{L_s}\right)$ into Eq. (13) and comparing with Eq. (14), the function of equilibrium contact angle combined the viscous effects of the wedge and bulk parts $c_3(\theta_e)$ is:

$$c_3(\theta_e) = 53.1\pi^{2/3}\left(\frac{\sin^3\theta_e}{2 \quad 3\cos\theta_e + \cos^3\theta_e}\right)^{1/3} c_1(\theta_e) + c_2(\theta_e) \tag{15}$$

The contact angle hysteresis is independent of the droplet size at the onset of motion. The advancing/receding contact angle can be assumed not to change much when droplet slides slowly. Therefore, $c_3(\theta_e)$ can be considered as a constant as well as $c_1(\theta_e)$ and $c_2(\theta_e)$.

Eq. (14) is a classic linear scaling law of moving droplet velocity in a low-velocity regime (Podgorski et al., 2001; Kim et al., 2002). Capillary number *Ca* linearly depends on Bond number *Bo* with its slope determined by the surface properties. Although this result is obtained through the approximate modeling, the linear relationship between *Ca* and *Bo* is suggested to estimate the steady sliding velocity of a water droplet on a specific surface in a low velocity regime. This conclusion is validated widely against the experimental data (Mannetje et al., 2014). The slope and intercept of the linear scaling law depend on the static advancing and receding contact angles.

2.3. Improvement of droplet velocity model

For the droplet velocity model at relatively high *Re* (*Re*≫1) number, the droplet internal flow field and the dynamic contact angles should be considered to estimate the viscous force and the surface tension force acting on the fast moving droplet. In addition, the Marangoni effect inside the droplet due to temperature gradient under condensation condition in nuclear comtainment can not be ignored. The equivalent Marangoni force here acting on moving droplet is valid for the whole velocity regime (both low and high *Re*). The proposed Marangoni force expression in our previous research (Wang and Cheng, 2019) is:

$$F_M = \Delta\sigma_{LG} \cdot \left[k \cdot 2r\left(\cos\theta_{d,R} \quad \cos\theta_{d,A}\right)\right] \tag{16}$$

The forces acting on a fast moving droplet are shown in Fig. 3. The force balance at the moving direction after considering the equivalent Marangoni force, is rewritten as:

$$F_g \sin\alpha = F_\sigma + F_{\tau,w} + F_\tau + F_M \tag{17}$$

The viscous force F_τ is determined by the velocity gradient inside the droplet. In case of droplet moving fast, the internal flow field of droplet seems to be a rotating flow field, as shown in Fig. 3 and zoomed in Fig. 4, blue part, which is usually observed both in experiments (Sakai et al., 2006; Song, 2008; Suzuki et al., 2008) and Computational Fluid Dynamics (CFD) simulations (Sikarwar et al., 2010). It is expected that the viscous force of the bulk part of the droplet is concentrated on the solid surface. The linear velocity gradient assumption of the moving droplet is no longer valid when the internal rotating flow field is considered. Meanwhile, the whole droplet has an average velocity (Fig. 4, yellow part) moving downwards.

A boundary layer with thickness δ occurs when a droplet moving fast on a solid surface. The height of this layer starts from the stagnant point in the droplet center, and ends to the solid surface. The real flow field in this boundary layer is the result of a rotating flow field overlapping on the average flow field. These two overlaid flow fields result in the final net flow field in the layer close to the solid surface, as shown in Fig. 4, red part. The layer thickness δ becomes thin with droplet speed increasing (Sikarwar et al., 2010). In this laminar boundary layer, the inertial force (per unit volume) is assumed as the same order of magnitude of viscous force (Schlichting, and Gersten, 2016), namely $\frac{\rho u^2}{\Delta y} \sim \mu\frac{u}{\delta^2}$. Therefore, the layer thickness can be closely approximated

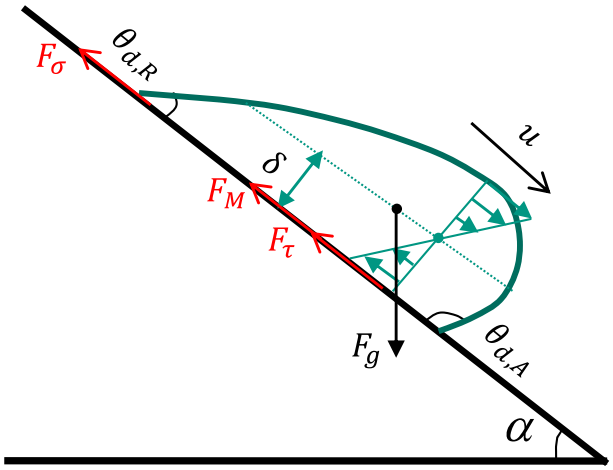

Fig. 3. Forces acting on moving droplet at high ***Re***.

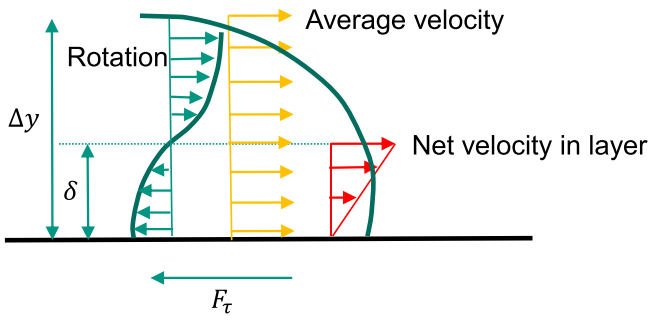

Fig. 4. Internal flow field of moving droplet.

by:

$$\delta \sim \frac{\sqrt{r\Delta y}}{\sqrt{Re}} \tag{18}$$

where ~ means 'of the order of'. The droplet Reynolds number is defined as $Re = \frac{\rho u r}{\mu}$. In reality, the shape of the droplet on the inclined wall is non-spherical. It varies with the surface properties and sliding velocity. However, in literature, e.g. the dropwise condensation papers (Rose and Glicksman,1973, Kim and Kim, 2011), the spherical cap is adopted to describe the droplet shape. Therefore, the droplet geometry model (spherical cap assumed, Meric and Erbil, 1998), as seen in the Eq. (9), is adopted to calculate the Re number.

The velocity gradient at the solid–liquid interface is approximated in this paper:

$$\frac{\partial u}{\partial y} \approx \frac{u}{\delta} = \frac{u\sqrt{Re}}{\sqrt{r\Delta y}} \tag{19}$$

Thus, the updating viscous force of the bulk part of droplet is:

$$F_\tau = \mu A \frac{\partial u}{\partial y} = \mu A \frac{u\sqrt{Re}}{\sqrt{r\Delta y}} = \mu u V^{1/3}\sqrt{Re}c_4(\theta_e) \tag{20}$$

Substituting the expressions of droplet geometry, i.e. the volume V, area A, radius r and height Δy into the above viscous force F_τ, the coefficient $c_4(\theta_e)$ can be obtained as a function of equilibrium contact angle:

$$c_4(\theta_e) = \frac{A}{V^{1/3}\sqrt{r\Delta y}} = \pi\left(\frac{3}{\pi}\right)^{1/3}\left(\frac{\sin^3\theta_e}{2 \quad 3\cos\theta_e + \cos^3\theta_e}\right)^{1/2}\left(\frac{2+\cos\theta_e}{1 \quad \cos\theta_e}\right)^{1/6} \tag{21}$$

The coefficient $c_4(\theta_e)$ is newly introduced in this paper comparing our previous studies (Wang and Cheng, 2019). Updating the knowledge of the viscous force F_τ in Eq. (20), the droplet velocity depending on droplet size can be derived by the following force balance:

$$\rho V g \sin\alpha = 2kr(\sigma_{LG}+\Delta\sigma_{LG})\left(\cos\theta_{d,R} \quad \cos\theta_{d,A}\right) + 4\mu u P c_1(\theta_e)\ln\left(\frac{L_a}{L_s}\right) + \mu u V^{1/3}\sqrt{Re}c_4(\theta_e) \tag{22}$$

Comparing with the previous model Eq. (12), the considered equivalent Marangoni force can be combined with surface tension force, which seems the Marangoni effect modifies the surface tension consequently. The viscous force F_τ is determined by the velocity gradient with the Re effect. If the droplet geometry is not sensitive to the slow sliding droplet, so that the dynamic advancing and receding contact angle can be replaced by static advancing and receding contact angle. However, for the fast moving droplet, the dynamic contact angle model should be adopted.

Non-dimensional parameters Bo_c and Re can be used to characterize the surface properties effect and viscous force on the droplet motion. Following the method in Eqs. (12) to (14) to nondimensionalize the force balance Eq. (22), both sides of the Eq. (22) divided by $\sigma_{LG}V^{1/3}$ and rearranged afterwards, one is obtained:

$$Ca\left(1 + c_5\sqrt{Re}\right) \propto Bo \quad c_6 \cdot \left(\cos\theta_{d,R} \quad \cos\theta_{d,A}\right) \tag{23}$$

Studies on the dynamic contact angles indicate they are monotonous with contact line velocity (Dussan, 1976; Voinov, 1976; De Gennes, 1985; Cox, 1986, 1998; Blake, 2006). The dynamic advancing contact angle increases, but the dynamic receding angle decreases with the growth of droplet velocity. There is a clear velocity dependence of these dynamic contact angles, which are determined by surface properties, i.e. the static contact angles. Many literature are reviewed in our previous paper (Wang et al., 2018) about the model of dynamic contact angles. The molecular kinetic model $\cos\theta_d \quad \cos\theta_s \propto f(Ca)$ indicates that the dynamic contact angles can be expressed as a function of the surface properties (static contact angles, namely the critical Bond number Bo_c,) and the Capillary number Ca. Therefore, the non-dimensional form of Eq. (22) is rewritten as:

$$Ca\left(1 + c_5\sqrt{Re}\right) \propto Bo \quad Bo_c f(Ca) \tag{24}$$

When the droplet slide very slowly ($Re < 1$), the dynamic contact angles can be replaced by the static and the Re effect can be negelected on viscous force. In this case, the result is the same with the scaling law of Eq. (14). In the calculation of this paper, a third order form is a typical model for droplet moving at a moderate speed (Voinov, 1976), which is usually adopted for dynamic contact angle evaluation $\theta_d^3 \quad \theta_s^3 \propto Ca$. The third order form predicts well the dynamic receding contact angle, since the variation of dynamic receding contact angles is not so large. However, Cox (1998) concludes the dynamic advancing contact angle is additinally influenced by the droplet Reynolds number, and emphasizes the inertia should not be ignored. The Cox (1998) model of the dynamic advancing contact angle considers the fluid inertial effect when droplets move at a high speed, namely the dynamic contact angle model includes the Re effect. The Cox model for predicting the advancing contact angle is expressed as:

$$Ca \cdot \ln\left(\frac{L_a}{L_s}Re^{-1}\right) = g_v(\theta^*) \quad g_v(\theta_{s,A}) \tag{25}$$

$$Ca \cdot \ln(Re) = g_{iv}(\theta_{d,A}) \quad g_{iv}(\theta^*) \tag{26}$$

where θ^* is an intermediate variable in the Cox model. The functions of contact angle are:

$$g_{iv}(\theta) = 1,53162(\theta \quad \sin\theta) \tag{27}$$

$$g_v(\theta) = \int_0^\theta \frac{\theta \quad \sin\theta\cos\theta}{2\sin\theta} \tag{28}$$

The subscript v and iv mean viscous and inviscid respectively. The definition Re number in Cox model is $Re = \frac{\rho u r}{\mu}$.

2.4. Transition criterion from droplet to rivulet

The flow pattern transition from droplet to rivulet is a very complicated process. The surface tension, which makes the droplet acquiring the least surface area, shapes the droplet structure. The transition criterion is proposed in our previous study (Wang & Cheng, 2019). We assume that the moving droplet is artificially separated into two parts. It is reasonable that there is a pair of action and reaction forces acting on the interface between these two parts. When the surface tension force at the interface is less than the required action force on the interface, the droplet structure will be stretched, which means the transition from droplet to rivulet starts. The transition droplet size can be obtained by solving the criterion (Wang & Cheng, 2019):

$$\rho\frac{V_t}{2}g\sin\alpha \quad 2r_t\mu\frac{\partial u}{\partial y} \quad r_t(\sigma_{LG}+\Delta\sigma_{LG})\cos\theta_e = 2r_t\sigma_{LG}\frac{\left(\frac{\theta_e}{\sin\theta_e} \quad \cos\theta_e\right)}{\theta_e+\sin\theta_e} \tag{29}$$

Meanwhile, for understanding of the transition process, a simplified transition criterion is derived in the form as Bond number, which however is determined eventually upon the equilibrium contact angle and surface tension (Wang & Cheng, 2019):

$$Bo_t = \frac{\rho V_t^{2/3} g\sin\alpha}{\sigma_{LG}} = \frac{4\frac{\left(\frac{\theta_e}{\sin\theta_e}-\cos\theta_e\right)}{\theta_e+\sin\theta_e} + 2\cos\theta_e\left(1+\frac{\Delta\sigma_{LG}}{\sigma_{LG}}\right)}{\left(\frac{\pi(2-3\cos\theta_e+\cos^3\theta_e)}{3\sin^3\theta_e}\right)^{1/3}} \tag{30}$$

The transition size V_t or r_t can be obtained easily by knowing Bo_t. Obviously the transition point is dependent on the equilibrium contact angle and fluid properties.

3. Experiment

In order to validate the improved velocity model of moving droplet and to investigate the dynamic contact angle hysteresis of water droplet moving on a typical containment structure surface and the transition from droplet to rivulet, new fundamental experiments are carried out.

3.1. Experiment setup

A fundamental experiment study on water droplet motion is conducted. The velocity, shape and the dynamic contact angles of moving droplets are measured via the videos recorded during the tests. The experiment device so-called DRISE (Drop and Rivulet on Inclined Surface Experiment) is set up by stainless steel plate coated with InOrganic Zinc-rich paint (IOZ, a decontamination paint used in containment shell surface), with a fixed dimension (length 85 cm × width 18.3 cm × thickness 1 cm) but with three various slope angles (32.5°, 60.9°, 83.3°). The experiment schematic is shown in Fig. 5. In order to change the slope angle of the plate, the upper end is supported by a pedestal of adjustable height.

Water droplets are generated from a burette (Eppendorf Research plus) onto the inclined plate. The volume range of the burette is 0.1–200.0 μL (error is ± 0.05 μL). The size of droplet selected depends on the experimental requirement and the repeatability of the droplet generated stably. A digital high-speed camera (MEMRECAM, IMAGE TECHNOLOGY) is used to visualize the side view of the droplets in sync at 100–10000 fps with a LED light source, while another camera recorded the top view videos at 120/240 fps, as shown in Fig. 5. The quantity of frames determines the camera recording time (almost 6–60 s), because the memory of the MEMRECAM camera is fixed at 8 Gigabytes. GXlink software connects the camera and the computer for the post-process of the videos. A ruler with minimum scale 0.5 mm is fixed on the area where the camera captures photos, which is an assistant to measure the velocity and the size of droplets. The properties, such as surface tension, viscosity and density are strongly dependent on the water temperature. In present experiments the water temperature is about 20-23℃.

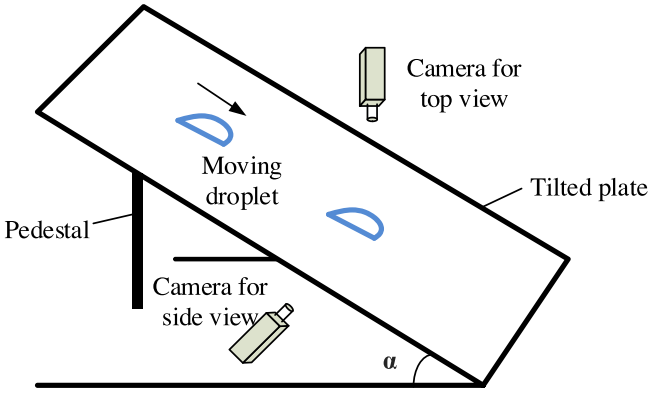

Fig. 5. Experimental schematic of droplet motion on tilted plate.

- Experiments Matrix

An overview of the parameters and test conditions is given in Table 2. $Ca = \mu u/\sigma_{LG}$ is the droplet capillary number with u being the droplet velocity, μ being the dynamic viscosity, and σ_{LG} being the surface tension of the water in the air. The Reynolds number $Re = \rho u r/\mu$ where r is droplet wetting area radius. The fluid properties at mean room temperature 21.5℃: surface tension σ_{LG}, 0.073 N/m; dynamic viscosity μ, 0.966 * 10^{-3} Pa*s; density ρ, 997.8 kg/m^3. Puthenveettil's experiment date will be used for model validation in section 4.

- Main Measurements

The slope angle of the steel plate from the horizontal is measured by a digital angle-measuring device with error<0.1°. Water droplet volume can be obtained by the droplet generator burette. Water temperature (here is the mean temperature of water surface and the inclined solid surface) is measured by infrared temperature gun.

The indirect measurements, e.g., the droplet velocity, the static/dynamic advancing and receding contact angles, are measured by post-processing of video records. The droplet velocity (an average from several frames) is the ratio of the droplet moving distance to the time passed between the selected frames. The static/dynamic contact angles of water droplets are measured between the tangents to the solid–liquid and the air–liquid interfaces in the zoomed side view images processed by an open source code ImageJ with a plugin DropAnalysis, as shown in Fig. 6. The contact angle reported here is the average value from several measurements at each velocity (including velocity = 0 for the static contact angles), with a measurement error about ± 3° due to the user effect of ImageJ.

3.2. Shape of moving droplet

When the droplet volume exceeds the critical volume (starting to move) on the surface with a specified inclination, the shape of the moving droplet could change with the droplet speed. The droplet contact area is no longer rounded but develops an ellipsoid at the rear with increase of droplet speed. The droplet shape is particularly easily discriminated by looking at the images recorded, as seen in Fig. 7. The evolution of water droplets moving on the surface with slope angle 83.3°, as shown in Fig. 8, indicates that the following three distinct shape regimes (oval or rounded, corner, cusp) can be identified during the evolution. A similar behavior is observed experimentally in references (Le Grand et al., 2005; Puthenveettil et al., 2013).

In Fig. 8, the Re numbers of the droplets are 65.7, 197.2 and 954.2 from left to right, the average velocities are 0.137, 0.0387, 0.159 m/s, and the radiuses are 4.67, 4.97, 5.47 mm respectively. The average static advancing and receding contact angles $\theta_{s,A}$ and $\theta_{s,R}$ are about 71.8° and 18.4° respectively. At different droplet velocity (obtained by changing the droplet volume while the surface inclination is fixed), the droplets adopt different shapes that are observed by recorded images. At low velocity, the droplet takes an oval shape. A corner develops at the rear with droplet velocity increasing further. The rear of the droplet is stretched by the effect of surface tension and viscosity, and then the corner shape goes to cusp. All these shapes transform quickly, in other words, these transitions take place in a short time. Finally, the rivulet occurs and its length of the contact line increases rapidly when the droplet volume increases beyond a threshold value.

The experiment uncertainty on the real paint IOZ coated stainless

Table 2
DRISE experiment campaign and comparison with Puthenveettil's experiment (Puthenveettil et al., 2013).

		V, μL	u, cm/s	$\theta_{d,A}$, °	$\theta_{d,R}$, °	Ca, 10^{-3}	Re	Data points
DRISE	Water	71.3–125.3	0.3–18	78–158	4–18	0.06–1.84	56–1700	8
Puthenveettil et al., 2013	Water	52.7 (g, mass)	3.8–59	108.8–121.7	47.6–73.4	0.3–7.5	137–3142	21
	Mercury	220 (g, mass)	7.2–23	150.6–161.4	94.6–144.6	0.23–2.3	2049–20069	16

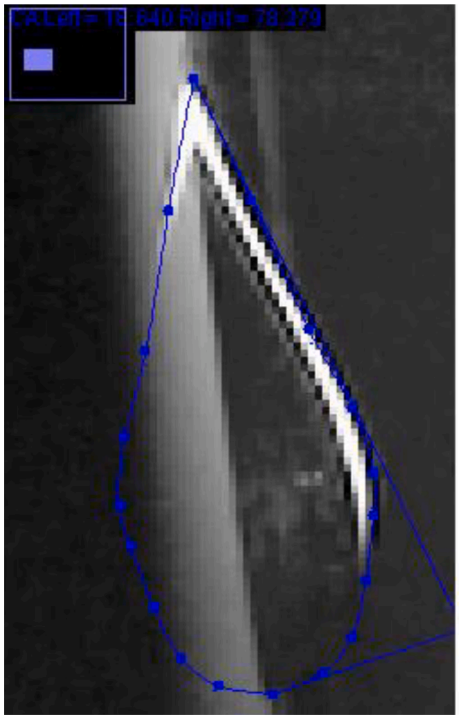

Fig. 6. Droplet contact angle measurement: static contact angles on surface with inclination of 83.3°.

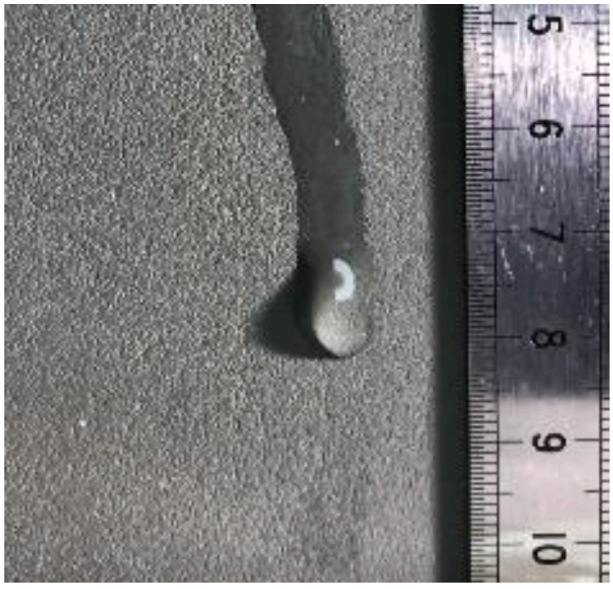

Fig. 7. Top view of the oval droplet with surface inclination of 32.5° (***Re*** 84.8).

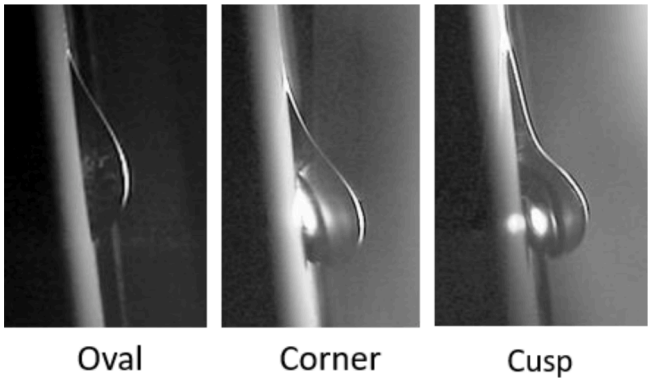

Fig. 8. Evolution of moving water droplet on surface with inclination of 83.3°.

steel surface is unavoidable. However, the following rules adopted in the experiment to get the data repeatedly: 1, before the experiment, the surface is cleaned with water as homogeneously as possible, 2, the identical droplet generates by burette on the same start-position, 3, the track of droplet motion keeps the same properties (dry surface with room temperature). The experiment of each data point, e.g. the velocity of moving droplet, is repeated at least 3 times. For the measurement of static contact angles, 9 times are repeated (3 × 3, repeated 3 times for each inclination angle).

Actually the high-speed camera has a quite small image field (around 5–10 times of the droplet diameter). The top view side camera has a relatively larger image field (above 6 cm long). Therefore, we don't record all the droplet moving track, but only the developed part of the trace. The top view side camera helps us to find the developed part intuitively at first, and many testes are done to confirm that by data analysis. The side view camera records are used to analyze the droplet velocity ultimately.

4. Model validation

4.1. Onset of droplet motion

In the present experiment, the non-uniformities in the paint layer on the steel surface results in heterogeneity, causing a contact angle hysteresis. Three tests have been done by increasing the droplet volume continuously to reach the threshold, beyond which droplets start moving with each specified inclination angle. The average static advancing and receding contact angles $\theta_{s,A}$ and $\theta_{s,R}$ of water droplets on the IOZ paint surface are measured at the onset of motion, which are about 71.8° and 18.4° respectively.

Meanwhile, wall inclination signifies the boundary of droplet volume over surface, which can be expressed as the critical Bond number

Table 3
Comparison of critical Bond number.

Inclination, α, °	Critical volume, V_c, μL	Critical Bond numbers,Bo_cExperiment	Calculation
32.5	55.9	1.0	0.88
60.9	24.8	1.01	1.18
83.3	22.4	1.07	1.07

Bo_c. The comparison of critical Bond number between the DRISE data and the theoretical prediction is carried out in Table 3. The critical droplet volume of motion increases with inclination angle decreasing, which can be conceived intuitively. The predicted critical Bond number Bo_c is calculated by the model of ElSherbini and Jacobi (2006), Eq. (4). Calculations are identical for water droplets on the specific homogeneous surface, which depend on the surface properties (i.e. the static contact angles), not on the surface inclination. Nevertheless, the increase of surface inclination leads to the decrease of critical droplet volume, as seen in Table 3. The comparison of critical Bond number Bo_c reveals that ElSherbini and Jacobi model is feasible to estimate the onset of motion of water droplets, despite large contact angle hysteresis (current case $\sim 50°$).

The deviation between the calculations is because the adopted contact angles are different from test to test. The gap between the DRISE data and the prediction of the model of ElSherbini and Jacobi might be caused by the measurement error of contact angles. The experimental critical Bond number $Bo_c = \frac{\rho V_c^{2/3} g \sin\alpha}{\sigma_{LG}}$ is calculated with the measurement of the inclination angle and the critical droplet volume (they are the values of the first and second column in Table 3 respectively). The error of the experimental critical Bond number is transmitted from the inclination and the critical droplet volume. The calculation of critical Bond number at the onset of motion Bo_c depends on the static advancing $\theta_{s,A}$and receding contact angles $\theta_{s,R}$, as shown in Eq. (4). Therefore, its error comes from the measurement uncertainty of the static contact angles.

4.2. Droplet velocity

4.2.1. Dynamic contact angle model

The droplet velocity model at low *Re*, takes the static contact angles into account for the surface tension, due to the assumed minor change of droplet shape. However, the geometry of the droplet changes dramatically when the droplet moves fast. Therefore, the dynamic contact angles should be considered in the droplet velocity model when droplet moves at high *Re*. The dynamic advancing contact angle model (Cox, 1998) that considers the inertial fluid effect when droplets move at a high speed, namely, the dynamic contact angle model includes the *Re* number effect.

Fig. 9 shows the comparison of the DRISE and Puthenveettil et al., 2013 experimental data with Cox (1998) model. The x-axis and y-axis represent the left and right sides of Eq. (26), respectively. The larger inclination and the larger volume are, the larger velocity of moving droplet, namely the larger *Ca* number and *Re* number are. The error bar of the x-axis $Ca\cdot\ln(Re)$ indicates one standard deviation of the uncertainty in the reported measurement, which mainly consists of the standard deviation of velocity u and the droplet radius r (transferred from contact angles). According to Cox model, the advancing contact angles of DRISE can be fitted linearly with a pre-factor of 219, which is two orders of magnitude higher than the expected from Cox's suggestion of one. Furthermore, Puthenveettil's data of water droplets can also be fitted linearly with a pre-factor of 5.7; the data of mercury droplets need a pre-factor of 47.8. Puthenveettil's data looks closer to the predictions of Cox model. Nevertheless, none of these three sets of data does coincide with the pre-factor of Cox's suggestion.

Therefore, in order to utilize a more common and generic empirical correlation instead of Cox model without a specific fitting factor for each case, a dynamic contact angle correlation is fitted by the present and Puthenveettil's experimental data:

$$\left(\cos\theta_{d,R} \quad \cos\theta_{d,A}\right) \quad \left(\cos\theta_{s,R} \quad \cos\theta_{s,A}\right) = 0.32We^{0.303}\left(1 \quad \cos\theta_e\right)^{-0.747} \tag{31}$$

where the Weber number $We = Ca\cdot Re$. Actually, *Ca* and *Re* number are used to fit the empirical correlation as well, results show both exponents of these two dimensionless parameters are close. Thus, *We* number works to fit against the experimental data. The correlation structure is proposed in terms of $\cos\theta_{d,R} \quad \cos\theta_{d,A}$ since this term is required in the droplet velocity model rather than the dynamic contact angels definitely. The prediction results are assessed by the DRISE and Puthenveettil's data, as shown in Fig. 10. The x-axis and y-axis represent the right and left sides of Eq. (31), respectively. It seems that all the experimental data agree with the generic correlation Eq. (31). It makes sense to approximate the dynamic contact angle hysteresis, which is feasible to be substituted into the improved droplet velocity model Eq. (22). The error bar of the x-axis (the combination of We number and θ_e) is in terms of the standard deviation of the velocity u and the equilibrium contact angle. The mean relative error between the data in DRISE experiment and the correlation predictions is around 35% due to the uncertainties of the measurements of droplet velocity and contact angles.

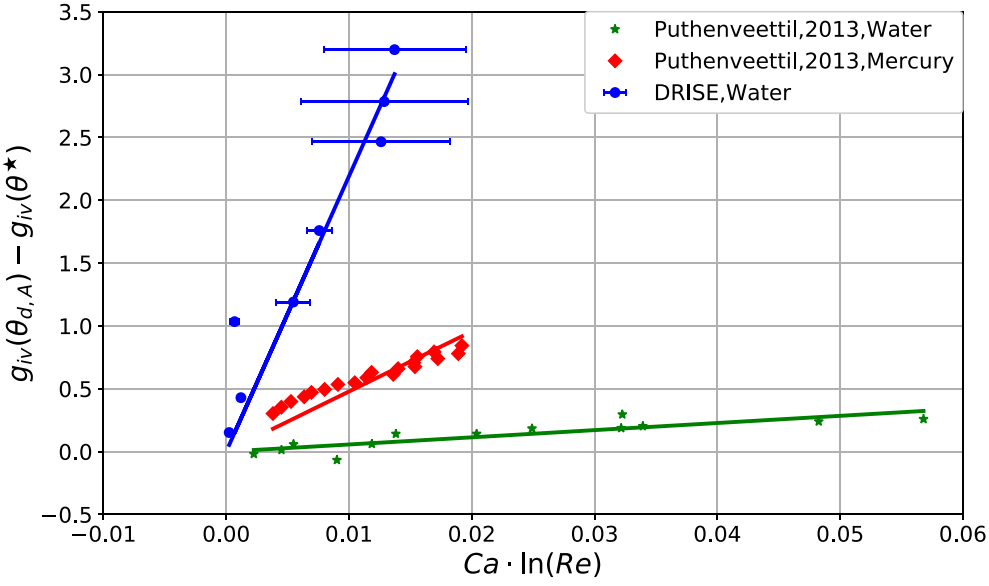

Fig. 9. Comparison of advancing contact angle with Cox, 1998 model.

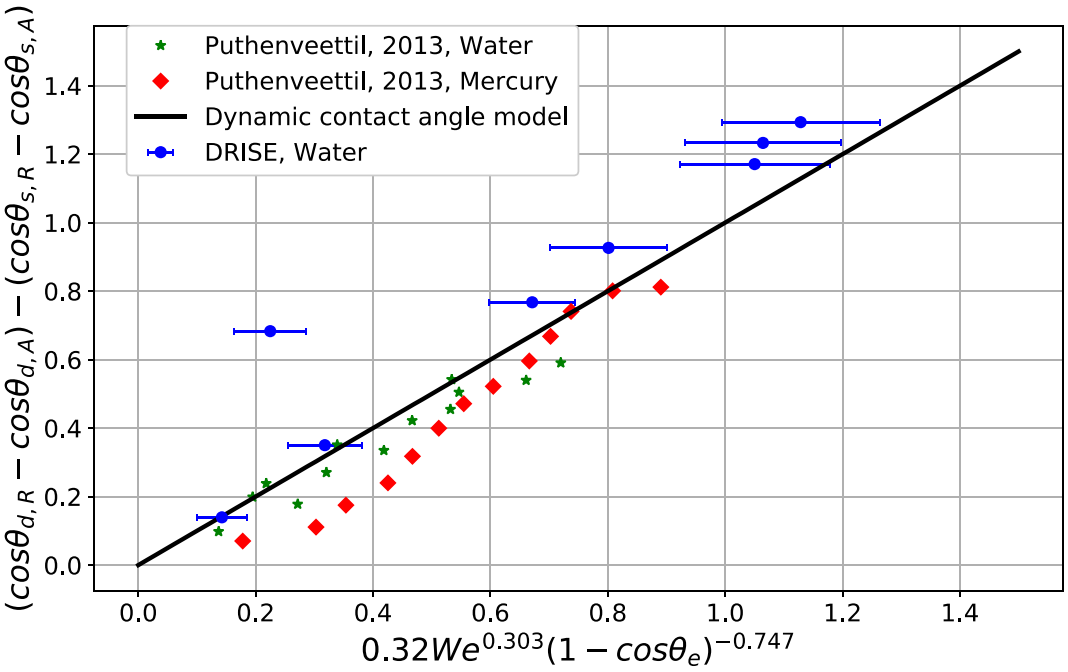

Fig. 10. Correlation of dynamic contact angle against experimental data.

4.2.2. Droplet velocity comparison

The dynamic contact angle hysteresis increases obviously with the droplet velocity. The new correlation of dynamic contact angle is adopted in the present model Eq. (22) to predict the droplet velocity. The surface tension as a resistance will therefore increase with droplet velocity apparently.

The equivalent Marangoni force is considered in the droplet force balance if there is a temperature gradient between the cold surface and bulk gas. Since there are no surface tension gradient in the current experiment and in Puthenveettil's experiment, the $\Delta\sigma = 0$ in the droplet velocity model.

The viscous force $F_{\tau,w}$ acts on the wedge part of droplet depends on the droplet size and the*Re*. The coefficient $c_1(\theta_e)$ of $F_{\tau,w}$ is derived by (Kim et al., 2002; Puthenveettil et al., 2013) based on the Stokes flow velocity field, which means $c_1(\theta_e)$ is only valid for small *Re* ($Re < 1$). In addition, the moving fast droplets usually have relatively larger droplet radius than the capillary length. Accordingly, the viscous force of the wedge part $F_{\tau,w}$ is neglected in the following comparison. However, the improved expression of F_τ (affected by *Re* number) is adopted in the present model Eq. (22) for droplet velocity assessment.

After substituting the improved expression of F_τ and the surface tension force F_σ (with dynamic contact angle model) into the force balance, the droplet velocity at high *Re* is obtained via the iteration of the implicit equation Eq. (22). The previous droplet velocity model Eq. (12) maintains static contact angles and the velocity gradient scaled to the ratio of the velocity and droplet height.

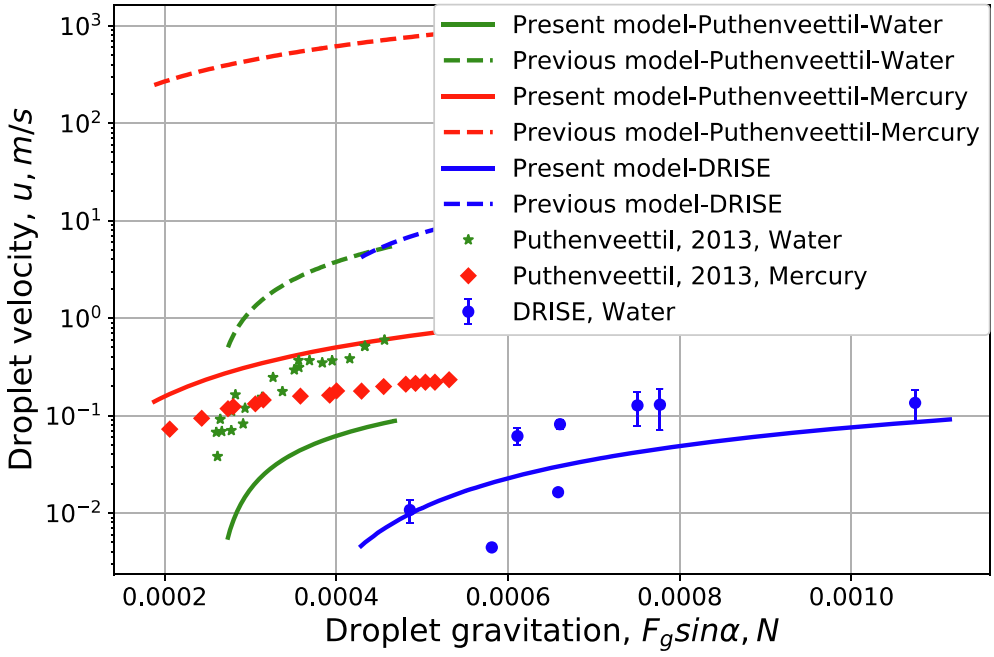

Fig. 11. Comparison of droplet velocity model against experimental data.

Fig. 11 shows the comparison between the model predictions and the experimental data. The increase of the droplet gravitation (coupling the inclination sin(α)) drives the increase of the droplet velocity. The comparison indicates the present model (the solid lines) has better predictions than the previous model (the dashed lines) since the shift of contact angles from the static to dynamic and the improvement of viscous force with effect of *Re* are considered in the present model. Both the shift of contact angles and the *Re* effect increase the resistance of droplet motion. The boundary conditions of Puthenveettil's experiment for the comparison are presented in Table 2. The fluid properties are obtained at mean room temperature 25 °C. The error bar of the y-axis is directly the droplet velocity standard deviation. The mean relative error between the data in DRISE experiment and the predictions is around 112% due to the heterogeneous of the wall surface.

4.3. Transition criterion

A few data points are obtained to validate the criterion of the transition from water droplet to rivulet. The purpose of the transition criterion is to determine the droplet size that leads to the transition happening. When the surface tension force at the interface between the droplet advancing and receding parts is less than the required action force on the interface, the structure will be stretched, which means the transition from droplet to rivulet starts. The transition droplet size V_t or r_t can be obtained by solving the criterion Eq. (29) via iteration and approximated by the proposed Bond number Bo_t in Eq. (30) at the transition point.

Fig. 12 shows the comparison of water droplet radius at transition point between the predictions and experimental data. The experimental data are generally in accordance with the predictions of the transition criterion. The transition droplet size obtained by solving the criterion via iteration are closer than the Bond number at the transition. The transition size (i.e. the Bo_t) of water droplet on glass (Puthenveettil's data,$\alpha = 90^{\circ}$) is less than on the decontamination paint. The reasons is the inclination is larger than the other data points on one hand. On the other hand, the resistance caused by surface tension on glass is less than on decontamination paint. Comparing the red point and the blue one, it reveals that the higher inclination results in smaller droplet transition size, which means the droplet on a more inclined surface reaches the transition point earlier. The error bar of the experimental data is directly the transition droplet radius standard deviation, which determined by the measurement uncertainty of the contact angles. The average relative error of all data points is about 13.9%, which is caused by the measurement uncertainty and the assumption adopted in the transition criterion model.

5. Conclusions

The behavior of moving droplet on inclined containment wall is of importance to evaluate condensation heat and mass transfer. The related models of droplet motion are presented and a new fundamental droplet experiment is conducted to validate the models.

The droplet onset of motion and the droplet velocity model at low *Re* number are described as the result of literature study. With respect to the fast moving droplet, the inside internal flow field and the dynamic contact angle model are considered to evaluate the viscous force and the surface tension force respectively. The improved viscous force demonstrates the inertial effect in the layer close to solid surface. The criterion proposed in our previous work describes the flow pattern transition from droplet to rivulet, which is to obtain the droplet transition size.

The new experiment of water droplets moving on inclined surface coated with decontamination paint, DRISE, is performed with the *Re* number range 56<*Re*<1700. The model for the onset of the droplet motion predicts very well the DRISE data. The comparison between the dynamic contact angle model (Cox model) and the experimental data indicates the necessity of the case-dependent factor, so that the fitting generic correlation is presented. At high *Re* number, the new developed droplet velocity model on the tilted surface and the criterion of the transition from droplet to rivulet are well validated with the data from the DRISE experiment and the experiment of Puthenveettil.

CRediT authorship contribution statement

Fangnian Wang: Conceptualization, Writing - original draft. **Meng Zhao:** Supervision, Writing - review & editing.

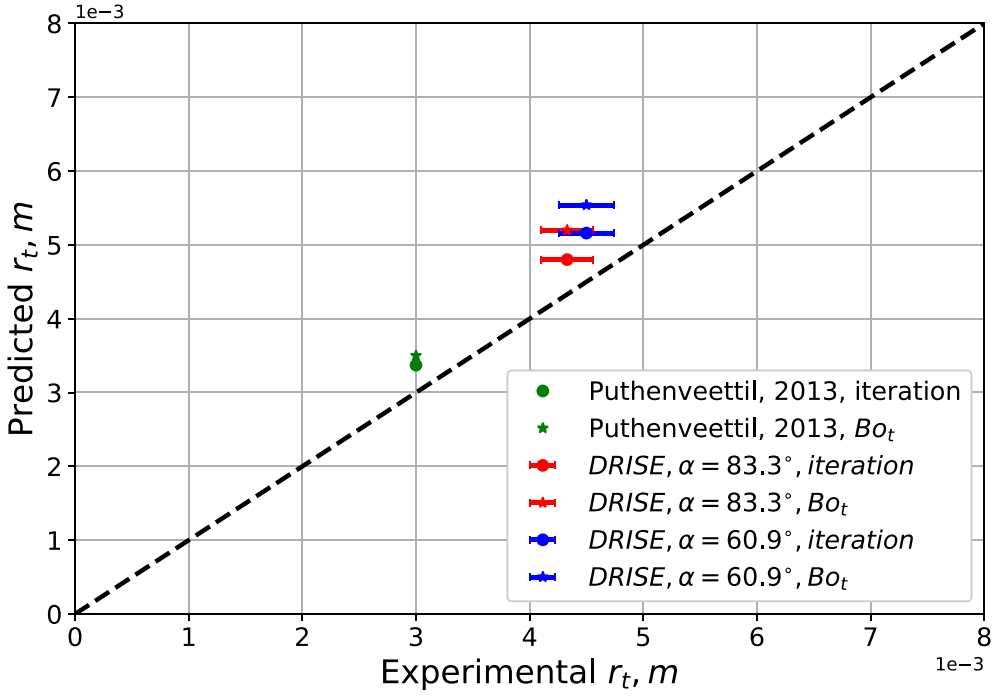

Fig. 12. Comparison of water droplet radius at transition point.

Declaration of Competing Interest

The authors declare that they have no known competing financial interests or personal relationships that could have appeared to influence the work reported in this paper.

Acknowledgments

This work is supported by the project "Erweiterung des Strömungsmodells zur Simulation des Aerosolabwaschens (ESSA, grant number:1501537)", funded by the German Federal Ministry of Economic Affairs and Energy (BMWi). We thank our partners Holger Norwack, Sara Beck from GRS and Sanjeev Gupta from Becker Technologies for many fruitful discussions. I also thank the financial support from china scholarship council (CSC, File Number: 201709110142).

References

Allen, R.F., Benson, P.R., 1975. Rolling drops on an inclined plane. J. Colloid Interface Sci. 50 (2), 250–253.

Blake, T.D., 2006. The physics of moving wetting lines. J. Colloid Interface Sci. 299 (1), 1–13.

Brown, R.A., Orr Jr, F.M., Scriven, L.E., 1980. Static drop on an inclined plate: analysis by the finite element method. J. Colloid Interface Sci. 73 (1), 76–87.

Cox, R.G., 1986. The dynamics of the spreading of liquids on a solid surface. Part 2 Surfactants. J. Fluid Mech. 168, 195–220.

Cox, R.G., 1998. Inertial and viscous effects on dynamic contact angles. J. Fluid Mech. 357, 249–278.

De Gennes, P.G., 1985. Wetting: statics and dynamics. Rev. Mod. Phys. 57 (3), 827.

J.C. De la Rosa A. Escrivá L.E. Herranz T. Cicero J.L. Muñoz-Cobo Review on condensation on the containment structures 2009 Nucl. Energy Prog 10.1016/j.pnucene.2008.01.003.

Dussan, E.B.V., 1985. On the ability of drops or bubbles to stick to non-horizontal surfaces of solids. Part 2. Small drops or bubbles having contact angles of arbitrary size. J. Fluid Mech. 151, 1–20. https://doi.org/10.1017/S0022112085000842.

Dussan E.B., V., 1976. The moving contact line: The slip boundary condition. J. Fluid Mech. 77, 665–684.

ElSherbini, A.I., Jacobi, A.M., 2006. Retention forces and contact angles for critical liquid drops on non-horizontal surfaces. J. Colloid Interface Sci. 299, 841–849. https://doi.org/10.1016/j.jcis.2006.02.018.

Extrand, C.W., Kumagai, Y., 1995. Liquid drops on an inclined plane: the relation between contact angles, drop shape, and retentive force. J. Colloid Interface Sci. 170 (2), 515–521.

Furmidge, C.G.L., 1962. Studies at phase interfaces. I. The sliding of liquid drops on solid surfaces and a theory for spray retention. J. Colloid Sci. 17 (4), 309–324.

Goodwin, R., Rice, D., Middleman, S., 1988. A model for the onset of motion of a sessile liquid drop on a rotating disk. J. Colloid Interface Sci. 125 (1), 162–169.

Kim, S., Kim, K.J., 2011. Dropwise condensation modeling suitable for superhydrophobic surfaces. J. Heat Transfer 133 (8).

Kim, H.Y., Lee, H.J., Kang, B.H., 2002. Sliding of liquid drops down an inclined solid surface. J. Colloid Interface Sci. 247, 372–380.

Le Grand, N., Daerr, A., Limat, L., 2005. Shape and motion of drops sliding down an inclined plane. J. Fluid Mech. 541, 293–315.

Mannetje, D., Ghosh, S., Lagraauw, R., Otten, S., Pit, A., Berendsen, C., Zeegers, J., van den Ende, D. and Mugele, F., 2014. Trapping of drops by wetting defects Nat.

Meric, R.A., Erbil, H.Y., 1998. Evaporation of sessile drops on solid surfaces: pseudospherical cap geometry. Langmuir 14, 1915–1920. https://doi.org/10.1021/la970147c.

Pierce, E., Carmona, F.J., Amirfazli, A., 2008. Understanding of sliding and contact angle results in tilted plate experiments. Colloids Surf., A 323 (1–3), 73–82.

Podgorski, T., Flesselles, J.M., Limat, L., Kim, H.Y., Lee, H.J., Kang, B.H., 2001. Sliding of liquid drops down an inclined solid surface. J. Colloid Interface Sci. 247, 372–380. https://doi.org/10.1103/PhysRevLett.87.036102.

Puthenveettil, B.A., Senthilkumar, V.K., Hopfinger, E.J., 2013. Motion of drops on inclined surfaces in the inertial regime. J. Fluid Mech. 726, 26–61. https://doi.org/10.1017/jfm.2013.209.

Rose, J.W., Glicksman, L.R., 1973. Dropwise condensation—the distribution of drop sizes. Int. J. Heat Mass Transf. 16 (2), 411–425.

Ryley, D.J., Ismail, M.S.B., 1978. The shape of sessile water drops on inclined plane surfaces. J. Colloid Interface Sci. 65 (2), 394–396.

Sakai, M., Song, J.H., Yoshida, N., Suzuki, S., Kameshima, Y., Nakajima, A., 2006. Direct observation of internal fluidity in a water droplet during sliding on hydrophobic surfaces. Langmuir 22 (11), 4906–4909.

Schlichting, H., Gersten, K., 2016. Boundary-Layer Theory. Springer.

Sikarwar, B.S., Muralidhar, K., Khandekar, S., 2010. Flow and Heat Transfer in a Pendant Liquid Drop Sliding on an Inclined Plane. In: In Proceeding of the 9th International ISHMT–ASME Heat and Mass Transfer Conference, pp. 1322–1329.

Song, F., 2008. Water droplet movements on methyl-terminated organosilane modified silicon wafer surfaces (Doctoral dissertation). University of Akron.

Suzuki, S., Nakajima, A., Sakai, M., Sakurada, Y., Yoshida, N., Hashimoto, A., Kameshima, Y., Okada, K., 2008. Slipping and rolling ratio of sliding acceleration for a water droplet sliding on fluoroalkylsilane coatings of different roughness. Chem. Lett. 37 (1), 58–59.

Takahashi, H., Higashino, Y., Sakai, M., Isobe, T., Matsushita, S., Nakajima, A., 2018. Sliding of water–glycerol mixture droplets on hydrophobic solid–liquid bulk composites using Ti plates with a fibrous TiO 2 layer. J. Mater. Sci. 53 (2), 1157–1166.

Voinov, O.V., 1976. Hydrodynamics of wetting. Fluid Dynam. 11 (5), 714–721.

Wadgaonkar, I.P., Sundararajan, T. and Das, S.K., 2015. Criterion for sliding/rolling characterization during droplet motion over superhydrophobic surfaces. arXiv preprint arXiv:1511.08563.

Wang, F., Cheng, X., 2019. Modeling approach of flowing condensate coverage rate on inclined wall for aerosol wash-down. Nucl. Eng. Des. 355 (2019), 110349.

Wang, F., Cheng, X., 2020. Extension and validation of aerosol wash-down model on inclined wall. Ann. Nucl. Energy 144, 107506.

Wang, F., Cheng, X., Köckert, L., 2018. Model assessment of condensate droplet motion on inclined containment structure surface. NUTHOS-12 1–13.